



NRC Publications Archive Archives des publications du CNRC

Numerical Simulation of the Effect of Processing Parameters on the Flow Behavior and Breakthrough Phenomenon in Co-Injection Molding Ilinca, F.; Héту, J. -F.

This publication could be one of several versions: author's original, accepted manuscript or the publisher's version. /
La version de cette publication peut être l'une des suivantes : la version prépublication de l'auteur, la version acceptée du manuscrit ou la version de l'éditeur.

Publisher's version / Version de l'éditeur:

Proceedings of the 21st Annual Meeting of the Polymer Processing Society(PPS-21), 2007, 2005-06-19

NRC Publications Record / Notice d'Archives des publications de CNRC:

<https://nrc-publications.canada.ca/eng/view/object/?id=b3b6339c-f9d4-4f66-93cf-3fee403ad3b8>
<https://publications-cnrc.canada.ca/fra/voir/objet/?id=b3b6339c-f9d4-4f66-93cf-3fee403ad3b8>

Access and use of this website and the material on it are subject to the Terms and Conditions set forth at

<https://nrc-publications.canada.ca/eng/copyright>

READ THESE TERMS AND CONDITIONS CAREFULLY BEFORE USING THIS WEBSITE.

L'accès à ce site Web et l'utilisation de son contenu sont assujettis aux conditions présentées dans le site

<https://publications-cnrc.canada.ca/fra/droits>

LISEZ CES CONDITIONS ATTENTIVEMENT AVANT D'UTILISER CE SITE WEB.

Questions? Contact the NRC Publications Archive team at

PublicationsArchive-ArchivesPublications@nrc-cnrc.gc.ca. If you wish to email the authors directly, please see the first page of the publication for their contact information.

Vous avez des questions? Nous pouvons vous aider. Pour communiquer directement avec un auteur, consultez la première page de la revue dans laquelle son article a été publié afin de trouver ses coordonnées. Si vous n'arrivez pas à les repérer, communiquez avec nous à PublicationsArchive-ArchivesPublications@nrc-cnrc.gc.ca.



Numerical Simulation of the Effect of Processing Parameters on the Flow Behavior and Breakthrough Phenomenon in Co-Injection Molding

F. Ilinca and J.-F. Héту

*Industrial Materials Institute, National Research Council,
75 de Mortagne, Boucherville, Qc, Canada, J4B 6Y4*

Abstract

In this work, a three-dimensional finite element flow analysis code is used to study the flow behavior during sequential co-injection molding. Non-Newtonian, non-isothermal flow solutions are obtained by solving the momentum, continuity and energy equations. Two additional transport equations are solved for tracking polymer/air and skin/core polymers interfaces. Solutions are presented for the filling of a spiral-flow mould for which experimental measurements are available. The numerical approach is shown to predict the core advance stage during which the core flow front catches up on the skin flow front and the core expansion phase when the flow fronts of core and skin materials advance together without breakthrough. The breakthrough phenomenon is also predicted and the numerical solution is in good agreement with the experiment. Those phenomena are hard to predict numerically and to our knowledge this is the first attempt at simulating the three-dimensional melt behavior during core expansion and core breakthrough. The predicted flow front behavior is compared to the experimental observations for various skin/core melt temperature, skin/core viscosity ratio, and core injection delay. Simulation results are in good agreement with experimental data and indicate correctly the trends in solution change when processing parameters are changing.

1 Introduction

The co-injection process has been known for about twenty years, since Garner and Oxley [1] first patented the process. Also known as sandwich molding, it consists basically in injecting in the mold cavity more than one plastic material to form a part with skin layers surrounding a core layer. The skin and core materials generally have different properties, but they must have a good adhesion at the interface, be processible in a comparable range of melt temperatures and present similar shrinkage characteristics. The first applications of the new process were in producing less expensive and lighter thick parts by using a foamed or recycled plastic for the core and a virgin plastic for the skin. Various other applications are in use today: skin or core made out of engineering resins to improve physical properties of the part such as strength, heat deflection or weather resistance, improvement of barrier properties of food containers, specifically multi-layer preforms for plastic bottles, and in-mold painting. The techniques of injecting the skin and core materials can be divided into two main methods: the one-channel technique which has a control valve that lets the melts enter the cavity in a sequential order [2], and the simultaneous injection which uses a two-channel nozzle [3]. The shortcomings of the one-channel technique (pressure drop and stagnation at the switchover point resulting in a 'hesitation line' having the shape of a dull ring) have been overcome by the two-channel technique, but the simultaneous injection is more difficult to control and require time-consuming trials.

Control of the flow fronts can be achieved by varying the core/skin ratio, processing conditions and rheological properties of the skin and core materials. Previous experimental studies on this subject dealt mostly with the role of the viscosity ratio of the two materials [4-7]. Few numerical simulations of the co-injection filling process have been attempted in the past decade [8-13]. All of them use the Hele-Shaw approximation to predict the interface evolution between skin and core material during filling for the sequential injection, with the exception of Lee et al. [12] who also considered the simultaneous injection. All these studies highlighted the importance of the viscosity ratio and the rate of injection. While for parts with non-uniform thick sections the Hele-Shaw approximation is clearly inappropriate, it is even more inaccurate in predicting the relative material distribution between the skin and core section. As the core

polymer penetration is a three-dimensional phenomenon, it is important to provide not only the depth of the core penetration, but also details on the core shape and polymer skin thickness. Flow instabilities due to a rheological mismatch between the skin and core materials can be difficult to predict and describe if one uses the Hele-Shaw approximation.

This contribution is an extension of our previous work on the three-dimensional simulation of the co-injection molding process [14-18]. The objective of this work is to investigate numerically the co-injection process in terms of the relative skin/core viscosity and temperature to gain further basic understanding of the flow behavior of two polymers during filling of a mold. The numerical approach provides the evolution of the polymer/air and core/skin interfaces and the final shape and depth of the core. The resolution of the true 3D mold-filling problem allows the computation of accurate and detailed information regarding the shape and the size of the core material, as well as the thickness of the skin. Those results are especially useful in critical regions such as near corners, obstacles, or in regions presenting changes in part thickness. A robust and accurate solution algorithm will also provide the framework for detailed analysis of the role played by different parameters determining the final characteristics of the part. In such a way the prediction of an optimal design of the process using simulation is a realizable task.

In this work we present solutions for a spiral-flow mold for which experimental measurements are available. The focus is on the numerical prediction of hard to simulate flow phenomena such as the core expansion phase during which the flow fronts of core and skin materials advance together without breakthrough. The breakthrough phenomenon is also predicted and the breakthrough point is compared with the experimental observation.

2 Model Equations

The equations governing the incompressible melt flow are the Stokes and continuity equations

$$0 = -\nabla p + \nabla \cdot (2\eta\dot{\gamma}(\mathbf{u})), \quad (1)$$

$$-\nabla \cdot \mathbf{u} = 0, \quad (2)$$

where $\dot{\gamma}(\mathbf{u}) = (\nabla\mathbf{u} + (\nabla\mathbf{u})^T) / 2$ is the strain rate tensor.

Heat transfer is modeled by the energy equation:

$$\rho c_p \left(\frac{\partial T}{\partial t} + \mathbf{u} \cdot \nabla T \right) = \nabla \cdot (k \nabla T) + 2\eta\dot{\gamma} : \dot{\gamma}. \quad (3)$$

In the above equations, t , \mathbf{u} , p , T , ρ , η , c_p and k denote time, velocity vector, pressure, temperature, density, viscosity, specific heat and thermal conductivity respectively.

The position of the polymer/air and skin/core polymer interfaces is tracked using a pseudo-concentration method [19]. The approach defines smooth functions $F_i(x, t)$ such that the critical value, F_c , represents the position of the interface. We consider $i=1$ for the polymer/air interface and $i=2$ for the skin/core interface. A front tracking value greater than F_c denotes a region filled by the respective polymer, while a smaller than F_c value corresponds to an unfilled region. As two interfaces are present the various combinations are summarized in Table 1. Front tracking solution identifies the skin, core and empty regions. Core breakthrough is also predicted.

Table 1: Definition of filled (skin/core) and empty regions

	$F_1 \geq F_c$	$F_1 < F_c$
$F_2 \geq F_c$	Core Polymer	Core breakthrough skin material
$F_2 < F_c$	Skin Polymer	Empty (air)

At each time step the pseudo-concentration function is obtained by solving a pure advection equation using the velocity field provided by the solution of the momentum-continuity equations:

$$\frac{\partial F_i}{\partial t} + \mathbf{u} \cdot \nabla F_i = 0 \quad \text{on } \Omega \quad (4)$$

Appropriate boundary conditions complete the statement of the problem. On the entry section both velocity and temperature are imposed. No-slip boundary conditions are imposed on the cavity walls filled by the polymer, while on the unfilled part, a free boundary condition allows for the formation of the typical fountain flow. The heat transfer between the cavity and the mold is given by

$$q_m = h_c (T - T_m) \quad \text{on } \Gamma_{\text{mould}}, \quad (5)$$

where h_c is a surface heat transfer coefficient and T_m is the mold temperature. For the front tracking functions, homogeneous Neumann boundary conditions are considered on all boundaries, except for the entry where Dirichlet conditions are imposed. Entry values change in time and indicate whether skin or core polymers are injected.

3 Finite element solution procedure

Model equations are discretized in time using a first order implicit Euler scheme. At each time step, the global system of equations is solved in a partly segregated manner. The solution algorithm solves separately the systems of equations as follows:

- [1]. Solve the incompressible momentum-continuity equations (\mathbf{u} - p).
- [2]. Solve the energy equation (T).
- [3]. Solve the front tracking equations (F_1, F_2).

When the skin polymer is injected, only the front tracking function for polymer/air interface (F_1) is solved, while during the core polymer injection both front tracking functions are computed. The finite element formulations of the equations are discussed hereafter.

The momentum-continuity equations (1) and (2) are solved using a Streamline Upwind Petrov-Galerkin (SUPG) method [20]. This method contains an additional pressure stabilization term compared with the standard Galerkin method. In such a way, the use of linear elements for both the velocity and pressure is permitted.

For polymers, the Prandtl number takes large values. Therefore, during the filling, the energy equation is dominated by the convection. However, cooling generated by the heat lost through walls, coupled with a low material diffusivity, determines apparition of high temperature gradients in direction normal to the wall. Hence, the solution algorithm must correctly represent both advective and diffusive mechanisms, which have highly different time scales. Here a GLS/GGLS stabilized finite element method is used [20,21]. The GLS method stabilizes for the convective term, while the GGLS formulation is designed to deal with thin boundary layers on materials having low conductivities. It reduces non-physical oscillations and improves the accuracy of the numerical solution.

The front tracking equations are discretized using a SUPG finite element method. SUPG provides smooth solutions when the convective part of the equation is dominant, as in the present case. The front tracking functions are discretized using linear elements. The functions F_1 and F_2 used to track the interfaces are reinitialized after each time step in order to improve their smoothness and to insure mass conservation of the skin and core polymers.

4 Material properties

The materials for this work are three different grades of polycarbonate: Panlite L-1225L (MFI=20) – low viscosity; Panlite L-1250 (MFI=8) – middle viscosity; Panlite K-1300 (MFI=3)

– high viscosity. Density, specific heat and thermal conductivity were considered constant, equal to 1200 kg/m^3 , $2000 \text{ J/(kg}\cdot\text{°C)}$, and $0.25 \text{ W/(m}\cdot\text{°C)}$ respectively. The viscosity was modeled by the Cross-WLF model equations

$$\eta = \frac{\eta_0}{1 + (\eta_0 \dot{\gamma} / \tau^*)^{1-n}} \quad (6)$$

$$\eta_0 = D_1 \exp\left\{ \frac{-A_1(T - T^*)}{A_2 + (T - T^*)} \right\} \quad (7)$$

where $T^* = D_2 + D_3 p$, and $A_2 = \bar{A}_2 + D_3 p$. The rate of deformation $\dot{\gamma}$ is computed from the strain rate tensor as $\dot{\gamma} = \sqrt{2\dot{\gamma}:\dot{\gamma}}$. Viscosity model constants used for the numerical simulation are summarized in Table 2.

Table 2: Cross-WLF model constants for the numerical modeling

Model constant	L-1225L	L-1250	K-1300
$n; \tau^* \text{ (Pa)}$	0.12; $8.5 \cdot 10^5$	0.12; $10.0 \cdot 10^5$	0.12; $12.0 \cdot 10^5$
$D_1 \text{ (Pa s)}; D_2 \text{ (°C)}; D_3 \text{ (°C/Pa)}$	$2.5 \cdot 10^9$; 175.0; 0.0	$10.5 \cdot 10^9$; 175.0; 0.0	$16.5 \cdot 10^9$; 175.0; 0.0
$A_1; \bar{A}_2 \text{ (°C)}$	22.0; 44.0	22.0; 44.0	22.0; 44.0

5 Numerical results

This application was the object of an experimental study by Watanabe et al. [24,25]. The mold has a spiral-flow cavity with 20mm width and 2mm thickness (see Figure 1). The melt is injected at 300°C and the mold is kept at 80°C. The core and skin materials were injected sequentially. The core material is injected at 0.7s when the flow length of skin material is about 30mm.

The position of skin and core materials at various times during the filling is shown in Figure 1 for the case when L-1225L was used as skin and core materials (S-L in Table 3). The skin material is plotted in transparency in order for the skin to be visible. As can be seen the core material advances more rapidly than the skin. As a result, the core catches up on the free surface of the skin material. The numerical solution for the skin and core flow lengths is compared with the experimental data of Watanabe et al. [25] in Figure 2. The numerical solution recovers the four experimentally observed regions of flow behavior:

- (I) Primary injection phase: only skin material is injected and skin flow front progresses inside the cavity.
- (II) Core advance region: the core material is injected and advances more rapidly than the skin, catching up on the free surface of the skin.
- (III) Core expansion region: once the flow front of core material catches up on the one of the skin material, the two flow fronts advance together without breakthrough.
- (IV) Core breakthrough region: only the core material is found on the free surface. Because the material from the free surface ends on the surface of the part, in the numerical simulation breakthrough is identified by the presence of the core material on the surface of the part.

The numerical model results in very accurate predictions and indicates correctly the core expansion phase between $t = 1.1\text{s}$ and $t = 1.4\text{s}$. The material behavior during this period is very hard to predict numerically since the flow front of core and skin materials advance together without breakthrough. To our knowledge this is the first numerical simulation approach dealing with this complex phenomena. Breakthrough occurs at about $t=1.4\text{s}$ close to the experimental observation. The numerical solution at the beginning of the core expansion phase and just prior to breakthrough is shown in Figure 3.

The flow behaviour of the skin and core materials was then analyzed for various temperatures and viscosities of the skin material. A summary of the simulations is shown in Table 3. The case of skin material with higher viscosity was simulated for skin temperatures of 300°C, 310°C and 320°C respectively (C-300, C-310 and C-320 in Table 3). Also computations were carried out for the cases for which materials with higher viscosity were used for the skin (S-M in Table 3 for skin with middle viscosity L-1250 and S-H for skin with high viscosity K-1300). Note that cases C-300 and S-H are the same.

Table 3: Summary of the molding conditions

Case	Skin temperature	Skin viscosity	Core temperature	Core viscosity
C-300	300	High	300	Low
C-310	310	High	300	Low
C-320	320	High	300	Low
S-L	300	Low	300	Low
S-M	300	Middle	300	Low
S-H	300	High	300	Low

Solutions for various temperatures of the skin material are compared with the experimental data in Figure 4. Simulations recover correctly the beginning of the core expansion phase but underestimate the length of the core expansion region especially for the case of skin material injected at 310°C as seen in Figure 5. However the numerical model correctly indicates an increase in the length of the core expansion region as the temperature of the skin material increases.

The solutions obtained for various skin viscosities are compared with the experiment in Figure 6. In this case the agreement with the experimental observations is much improved. The length of the core expansion region agrees well with the measured values as shown in Figure 7. For skin materials having a higher viscosity the breakthrough occurs sooner and the core expansion region is shorter. These results are in good agreement with the observations of Watanabe et al. [25].

6 Conclusion

This work presents a three-dimensional finite element method for solving the co-injection molding process. The procedure provides the evolution of the polymer/air and skin/core polymer interfaces and the final shape and depth of the core polymer. Solutions were presented for a spiral mold for which experimental data is available.

The proposed procedure is able to predict the core expansion phase, the core advance phase and the core breakthrough. It deals with changes in part thickness or flow direction, and provides all the needed information concerning skin thickness and core shape. It works in the same manner for thin parts and for thick three-dimensional parts.

Solutions for the spiral mold indicate a very good agreement between the numerical results and the experimental observations. Notably, the simulation predicts correctly the beginning of the core expansion phase (the moment when the core material catches up on the front of skin material) and the occurrence of core breaking through the skin. The influence of the material viscosity ratio and of the skin/core temperature is well recovered by the numerical simulation.

7 References

1. Garner P.J., Oxley D.F., British Patent No.1,156,217 (1971).
2. Sandiford, D.J.H., Oxley D.F., *Serving up a new plastics sandwich*, SPE J., 27, p. 39 (1971).

3. Eckardt H., *How to develop a successful coinjection application*, Proc. 14th Annual Structure Foam Conference, SPI ed. (1986).
4. White J.L., Dee H.B., *Flow Visualization for Injection Molding of Polyethylene and Polystyrene Melts*, Polym. Eng. and Sci., 14, No.3, (1974).
5. Young S.S., White J.L., Clark E.S., Oyanagi Y., *A Basic Experimental Study of Sandwich Injection Molding with Sequential Injection*, Polym. Eng. and Sci., 20, No.12, (1980).
6. White J.L., Lee B.L., *An experimental Study of Sandwich Injection Molding of Two Polymer Melts Using Simultaneous Injection*, Polym. Eng. and Sci., 15, No.3, pp. 233 (1993).
7. Chen C., Hsu K.F., Jung W.R., *Study of Polymer Melt Flow During Injection Molding Using Co-Injection Molding Technique*, SPE-ANTEC Tech. Papers, pp. 671 (1994).
8. Turng L.S., Wang V.W., Wang K.K., *Numerical Simulation of the Co-Injection Molding Process*, ASME HTD-Vol.175/MD-Vol.25, Heat and Mass Transfer in Solidification Processing, 113 (1991).
9. Turng L.S., Wang V.W., Wang K.K., *Numerical Simulation of the Coinjection Molding Process*, Trans. of the ASME – J. Engng. Mat. Tech. 115, p. 48 (1993).
10. Chen S.C., Hsu K.F., *Numerical Simulation and Experimental Verification of Melt Front Advancements in Coinjection Molding Process*, Num. Heat Transfer A, 28, p. 503 (1995).
11. Schlatter G., Davidoff A., Agassant J.F., Vincent M., *Numerical Simulation of the Sandwich Injection Molding Process*, SPE-ANTEC Tech. Papers, p. 456 (1995).
12. Lee D.J., Isayev A.I., White J.L., *Simultaneous Sandwich Injection Molding: Simulation and Experiment*, SPE-ANTEC Tech. Papers, p. 346 (1998).
13. Schlatter G., Davidoff A., Agassant J.F., Vincent M., *An Unsteady Multifluid Model: Application to Sandwich Injection Molding Process*, Polym. Eng. and Sci., 39, No. 1, p. 78 (1999).
14. Ilinca F., Héту J.-F., *Three-dimensional numerical modeling of co-injection molding*, PPS-17, 17th Annual Conference of the Polymer Processing Society, 12p., (2001).
15. Ilinca F., Héту J.-F., *Three-Dimensional Simulation of Multi-Material Injection Molding: Application to Gas-Assisted and Co-Injection Molding*, Pol. Eng. and Sc., 43, pp. 1415-1427 (2003).
16. Ilinca F., Héту J.-F., *Three-dimensional numerical modeling of co-injection molding*, International Polymer Processing Journal, 17:3, pp. 265-270 (2002).
17. Ilinca F., Derdouri, A., Héту J.-F., Messaoud, D.A., Sanchagrín, B., *Numerical Simulation and Experimental Validation of the Filling Stage in the Co-injection Molding Process*, SPE-ANTEC Tech. Papers, pp. 627-631 (2003).
18. Ilinca F., Héту J.-F., Derdouri, A., *Experimental and Numerical Investigation of the Flow Front Behavior in the Co-injection Molding Process*, PPS-18, 19p. (2002).
19. Ilinca F., Héту J.-F., *Three-dimensional filling and post-filling simulation of polymer injection molding*, Int. Polym. Process. 16, p. 291 (2001).
20. Franca L.P., Frey S.L., *Stabilized finite element methods: II. The incompressible Navier-Stokes equations*, Comp. Meth. Appl. Mech. Engng. 99, p. 209 (1992).
21. Franca L.P., Dutra do Carmo E.G., *The Galerkin Gradient Least-Squares Method*, Comp. Meth. Appl. Mech. Engng. 74, p. 41 (1989).
22. Ilinca F., Héту J.-F., Derdouri A., Holmes B., Scott C., Stevenson J., *Metal Injection Molding: Simulation of three-dimensional flow with free surface boundary and experimental comparison*, SPE-ANTEC Tech. Papers, p. 718 (2000).
23. Ilinca F., Héту J.-F., *Three-dimensional finite element solution of gas-assisted injection molding*, Int. J. Num. Methods Engng. 53, p. 2003, (2002).
24. Watanabe D., Ishiaku U.S., Nagaoka T., Tomari K., Hamada H., *Flow behavior of sandwich injection molding in sequential and simultaneous injection*, Int. Pol. Proc., 18:2, pp. 199-203 (2003).
25. Watanabe D., Ishiaku U.S., Nagaoka T., Tomari K., Hamada H., *The flow behaviour of core material and breakthrough phenomenon in sandwich injection molding*, Int. Pol. Proc., 18:4, pp. 405-411 (2003).

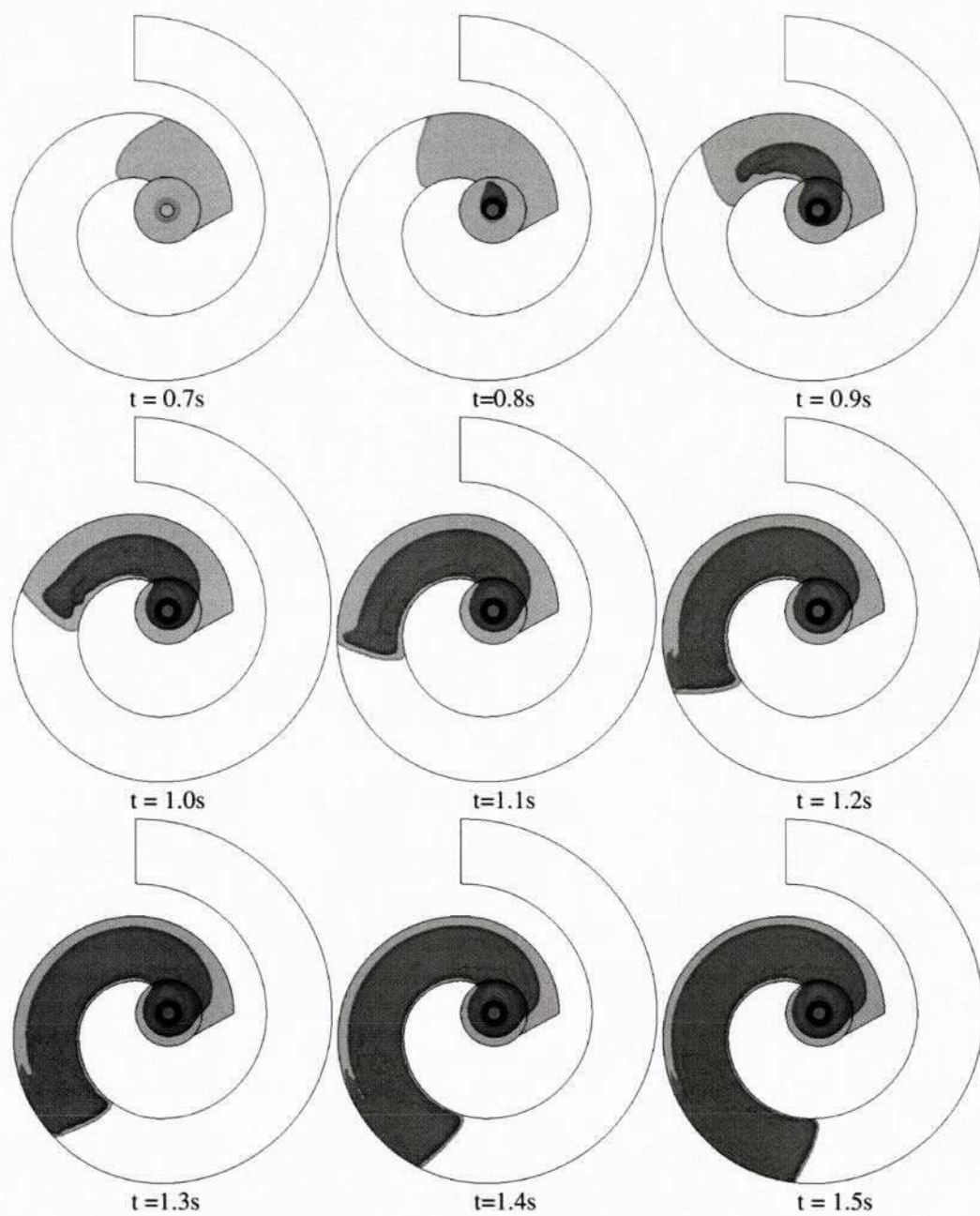


Figure 1: Spiral mold: evolution of the core penetration.

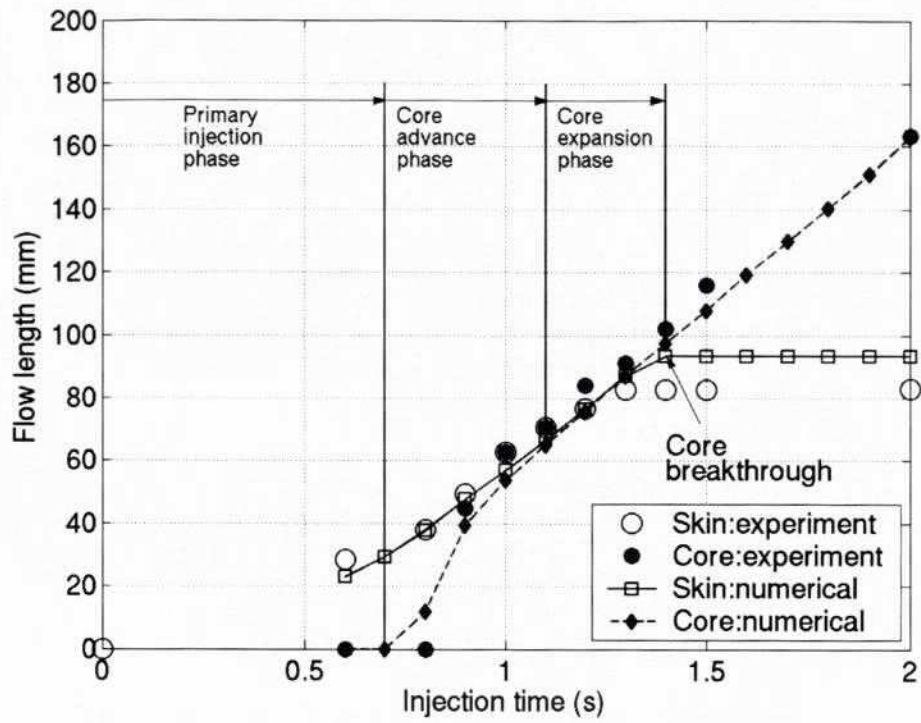


Figure 2: Skin and core position for spiral mold.

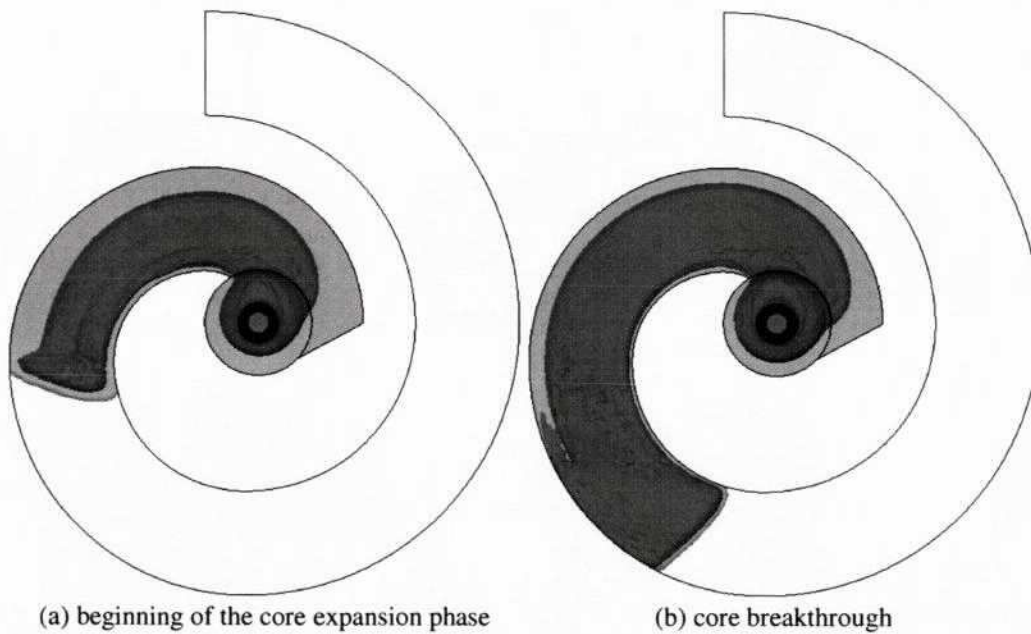
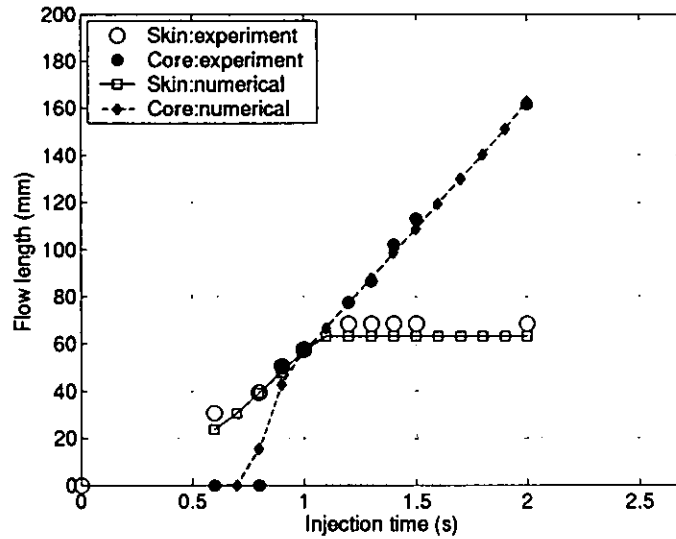
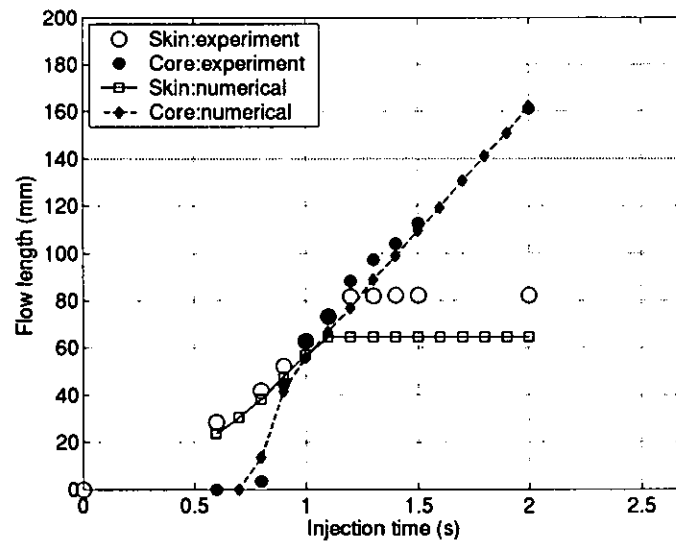


Figure 3: Core penetration: (a) beginning of the core expansion phase ($t=1.1s$), (b) breakthrough (end of the core expansion phase, $t=1.4s$).

(a) Skin temperature = 300°C



(b) Skin temperature = 310°C



(c) Skin temperature = 320°C

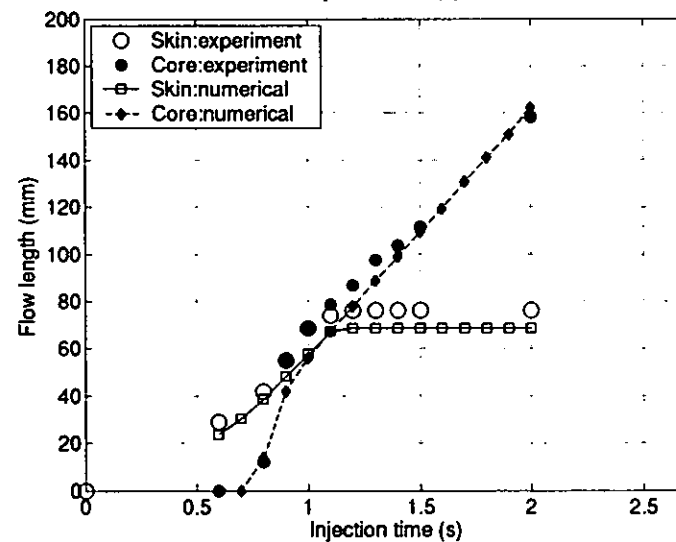


Figure 4: Relationship between flow length of skin/core material and injection time for various temperatures of skin material.

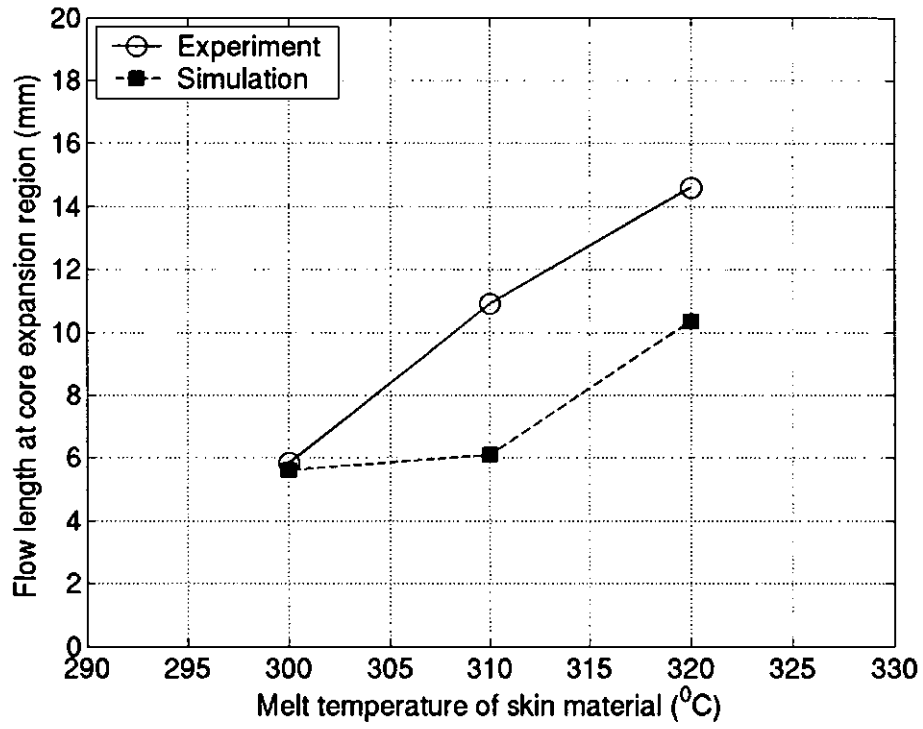
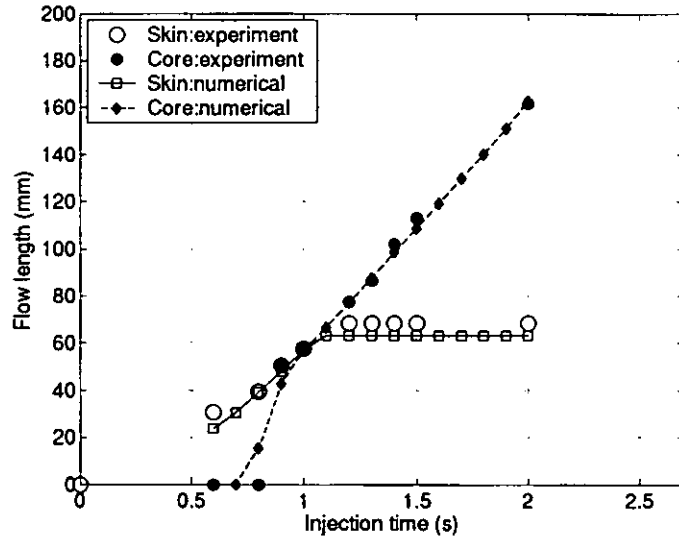
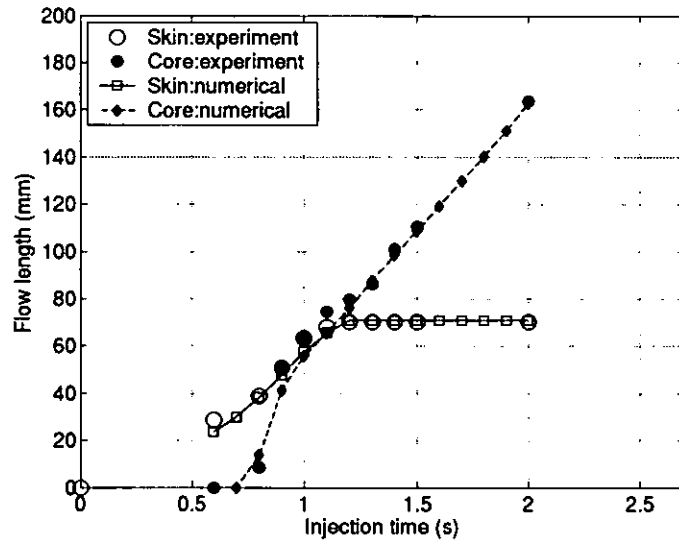


Figure 5: Relationship between flow length at core expansion region and the melt temperature of skin material.

(a) Skin viscosity = high



(b) Skin viscosity = middle



(c) Skin viscosity = low

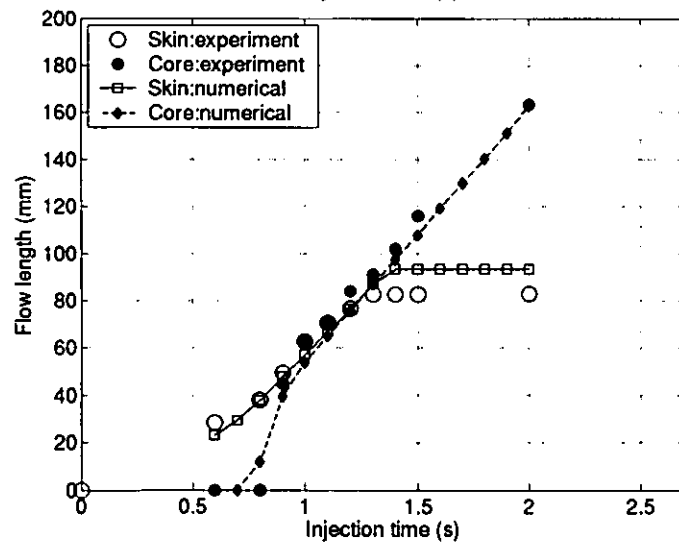


Figure 6: Relationship between flow length of skin/core material and injection time for various skin material viscosity.

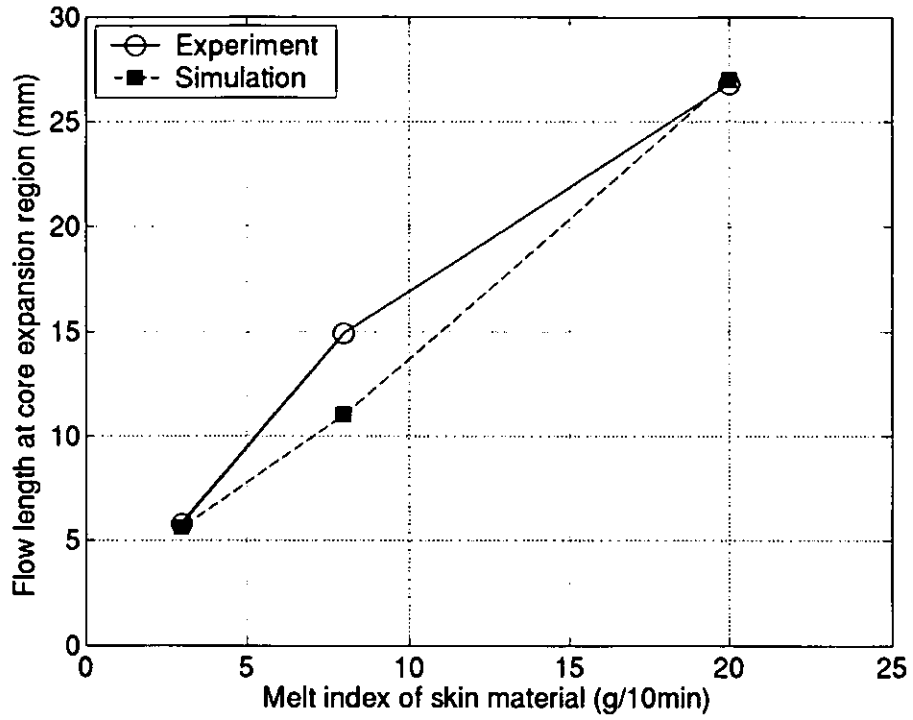


Figure 7: Relationship between flow length at core expansion region and the viscosity of skin material.